

Experimental Verification of Overcoming the Diffraction Limit with a Volumetric Veselago-Pendry Transmission-Line Lens

Jiang Zhu and George V. Eleftheriades

*The Edward S. Rogers Sr. Department of Electrical and Computer Engineering, University of Toronto,
10 King's College Road, Toronto, Ontario, Canada M5S 3G4*

(Received 4 January 2008; revised manuscript received 21 May 2008; published 2 July 2008)

A fully printed Veselago-Pendry lens (isotropic $n = -1$, $\epsilon_r = -1$, $\mu_r = -1$) is presented which is based on transmission-line metamaterials. The lens is constructed in a parallel-plate environment at 1.569 GHz and without any embedded sources and achieves a resolution better than the diffraction limit (full width half power of 0.235λ). Because the lens is low loss (<0.3 dB per unit cell), the focused fields are dominated by the evanescent components which dictates that subwavelength tightening of the beam is achieved only in the transverse and not the longitudinal direction. The demonstrated lens is quarter-wavelength thick thus allowing ample “working distance” between the subject/image and the lens.

DOI: 10.1103/PhysRevLett.101.013902

PACS numbers: 78.20.Ci, 41.20.Jb, 42.25.Fx

One of the most intriguing propositions of emerging negative-refractive-index (NRI) metamaterials is to overcome the diffraction limit using a Veselago-Pendry lens [1]. This lens is made out of an isotropic NRI slab having a refractive index equal to -1 (but with $\epsilon_r = -1$ and $\mu_r = -1$) and overcomes the diffraction limit by accessing transverse wave numbers $k_t > k_o$ through the resonant amplification of evanescent waves. Despite being proposed a few years ago, its physical realization has only been partially demonstrated because of the stringent material requirements that are needed, namely, low material losses, isotropy with an index very close to $n = -1$, and low mismatch losses [2,3].

In particular, the Veselago-Pendry lens was implemented in the quasistatic limit where the electrical “working distance” between the source and/or the image and the lens is extremely small [4–7]. Short working distances and/or high transmission losses are limiting attributes of recent negative-refraction subwavelength imaging structures using anisotropic or higher than $|-1|$ index slabs [8–10]. Some early success with quarter-wavelength thick Veselago-Pendry planar lenses has been reported using transmission-line based metamaterials [11] which are characterized by low losses and wide bandwidths due to the tight coupling between adjacent resonators [12]. Recently this transmission-line approach has been extended for making three-dimensional lenses [13]. However, both [11,13] have used embedded sources and the resulting image has also been embedded within the lens structure. Unfortunately, this limits the practical applications of these lenses and raises conceptual questions whether a transmission-line based Veselago-Pendry lens can be realized in practice to interact with sources that lie outside of the lens structure. Moreover, both structures [11,13] utilized chip lumped-elements to render their unit cells deeply subwavelength, which is an essential requirement for achieving subwavelength resolution [14]. Therefore, the question still remains of whether the transmission-line approach can be extended to construct Veselago-Pendry

lenses that can interact with nonembedded sources and whether such lenses can be made without any chip elements (i.e., fully printed). In this Letter we present such a fully printed transmission-line based Veselago-Pendry lens in a parallel-plate environment. The lens is quarter-wavelength thick like its planar predecessor [11] thus offering ample “working distance.”

The main idea behind the hereby presented Veselago-Pendry lens is to stack layers of the so-called “shunt node” of a negative-refractive-index transmission-line medium [15] upon one another to build up a volumetric metamaterial [16]. This “stacked” topology can be thought of as an ordinary 2D NRI-TL metamaterial [15] but with an additional ground plane above it to account for the stacking process. As pointed out in [17,18], the additional ground plane introduces a parallel-plate waveguide (PPW) parasitic mode between the two grounds, which couples to the desired backward propagation mode. To eliminate this parasitic mode, an additional asymmetric shorting upper via, connecting the microstrip line to the upper ground plane, is applied as shown in Fig. 1 [16].

The microstrip is printed on a Rogers RT/duriod 5880 ($\epsilon_r = 2.2$, $\tan\delta = 0.0009$) substrate with thickness of 3.175 mm (125 mil) and 0.5-oz (17 μm) standard copper cladding. The printed elements employ interdigital capacitors and spiral inductors as shown in Fig. 2. The smallest feature size is 0.2 mm, which is the finger width of the

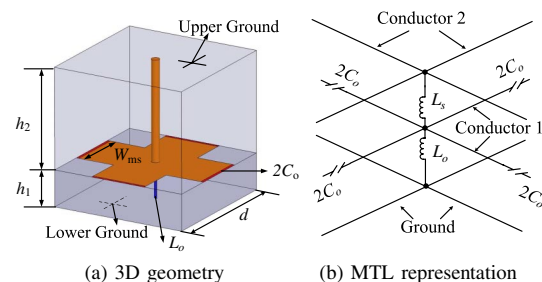


FIG. 1 (color online). Volumetric NRI-TL unit cell.

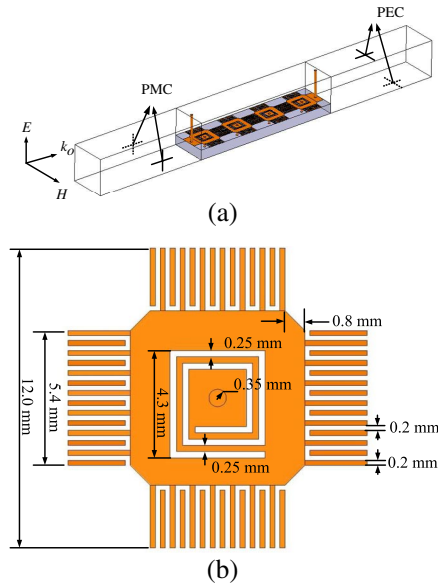


FIG. 2 (color online). Volumetric shunt-node NRI-TL slab shown in (a) and the printed features shown in (b).

interdigital capacitor. Each capacitor consists of seven finger pairs, contributing to a 0.9 pF capacitance. The spiral inductor has 5/4 turns with a turn width of 0.25 mm and is connected to the ground through a via. Combined with the shorting via, the spiral inductor provides about 8 nH inductance. Shorting metallic pins connecting the microstrip line to the upper ground have a radius of 0.35 mm and provide a parasitic inductance on the order of 3 nH. They are only placed at the input and output faces of the slab instead of at each unit cell in [16]. Because the slab is not excessively thick ($\lambda/4$), the PPW mode is still eliminated. At the same time, the fabrication process of the slab is greatly simplified. Furthermore, the unit cell has a dimension of $d \times d \times d = 12 \times 12 \times 12$ mm.

The simulation of the transmission magnitude for a normally incident vertically polarized plane wave is performed for a metamaterial slab consisting of four unit cells using the multiconductor transmission line (MTL) method [16,18] and the finite-element method full-wave electromagnetic solver Ansoft HFSS. Perfect E walls and perfect H walls are applied to the top and bottom walls, and side walls, respectively, to create an infinitely large metamaterial in the transverse direction. In Fig. 3(a), HFSS results demonstrate a -10 dB passband existing from 1.45 to 1.68 GHz, whereas the insertion loss is ranging from -1.0 to -1.2 dB, corresponding to 0.25 to 0.30 dB loss per unit cell (as opposed to the >2 dB loss per unit cell recently reported in [10]). Two resonances occur at 1.62 and 1.48 GHz, accounting for a 0° and 180° phase delay of the four cell metamaterial slab, respectively. The electrical length of the unit cell at the passband frequencies is on the order of $1/15$ free space wavelength, which makes the effective medium assumption valid. The effective ϵ and μ are extracted from the S parameters. As shown in

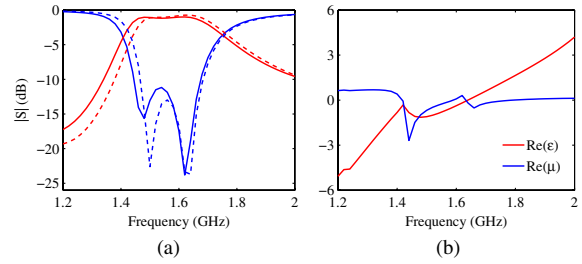


FIG. 3 (color online). Simulated transmission coefficient (red or gray lines) and reflected coefficient (blue or dark gray lines) from full-wave finite-element method solver Ansoft HFSS (solid lines) and the MTL theory (dotted lines) shown in (a) and the extracted effective material parameters ϵ and μ from S parameter, shown in (b).

Fig. 3(b), the real part of the extracted effective ϵ and μ are flat and close to -1 at the frequencies around 1.5 GHz (the real part of the refractive index $n' = -1.0 \pm 0.2$ and the imaginary part $n'' = -0.07 \pm 0.01$), which makes it suitable for super resolution lens application. It is worthwhile to notice the field distribution of the designed metamaterial slab at the operating frequency 1.50 GHz. Figure 4 shows the side view plot of the magnitude of the electric field along the plane crossing the central line of symmetry. Although the entire volume of the metamaterial slab is illuminated by the free space excitation, the electric field is highly confined within the substrate and the PPW mode is sufficiently suppressed by the upper vias placed at the input and output faces of the metamaterial slab.

The designed NRI-TL slab consists of one layer of 21×4 fully printed unit cells with the overall size ($w \times t \times h$) of $252 \times 48 \times 12$ mm, as shown in Fig. 5(a). The upper ground utilizes the bottom side of a double-sided Rogers RT/duriod 5870 ($\epsilon_r = 2.33$) substrate with thickness of 0.787 mm (31 mil) and is connected to the microstrip line through shorting pins. The slab lens is inserted into a parallel-plate waveguide (PPW) formed by two 70×49 mm printed circuit boards (PCB). It should be noted that although only one layer of the proposed NRI-TL lens is employed in the focusing experiment, the PPW duplicates an infinitely large number of such layers in the vertical dimension according to “image theory,” which effectively reproduces the required “stacking” process.

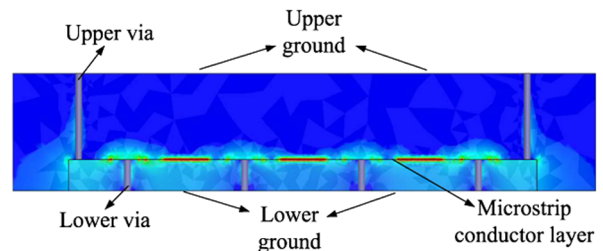


FIG. 4 (color online). Side view plot of the magnitude of the electric field along the plane crossing the central line of the NRI-TL metamaterial slab at 1.50 GHz. The electric field is highly confined within the substrate.

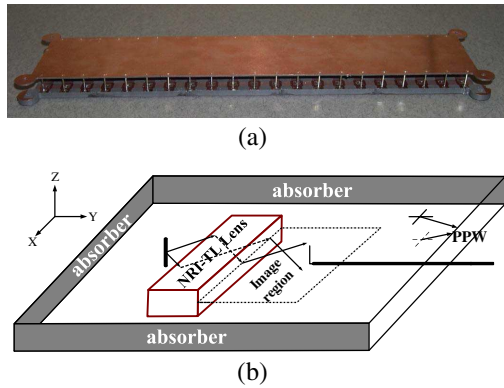


FIG. 5 (color online). The fabricated one layer shunt-node NRI-TL slab lens, consisting of 21×4 fully printed unit cells, as shown in (a) and the demonstration of the focusing experiment setup shown in (b).

The spacing between the PCBs is adjusted such that they tightly touch the upper and lower grounds of the slab. A monopole connecting to port 1 of an Agilent E8364B performance network analyzer (PNA) through a coaxial cable feeds the parallel-plate waveguide and illuminates the front side of the slab at a distance of 24 mm (two unit cells size) away from the lens. The parallel-plate waveguide is terminated by absorbers with one side left open. A probe made from a 1.19 mm-diameter semirigid coaxial cable is inserted into the PPW to sample the vertical electric field in the horizontal plane at the rear side of the lens, shown as the image region. It is positioned by a computer-controlled *xyz*-translator apparatus and connected to port 2 of the PNA. The whole experiment setup is shown in Fig. 5(b).

The scan takes 1 mm increment in both transverse and propagation directions. The best focusing results occur at 1.569 GHz, where the operating frequency is slightly higher than the designed frequency of 1.50 GHz. The plots of the field distribution at the frequency of 1.569 GHz are shown in Fig. 6. The measured vertical electric field is normalized to its maximum field value, occurring at the exit face of the lens, which indicates the enhancement of the evanescent waves in magnitude. The light spots, clearly seen at the transverse plane close to the lens, indicate the high intensity electric field. They correspond to the positions where the output upper vias lie. These measurements reasonably agree with the full-wave simulations from Ansoft HFSS shown in Fig. 1 in the supplementary material [19]. The presence of strong evanescent waves at the exit interface of the lens can be inferred from the phase plot in Fig. 7(a) and more apparently in Fig. 7(b). Indeed the least phase progression is observed at the interface between NRI-TL lens and free space, where the evanescent waves dominate. With increasing the distance away from the lens, the phase progression becomes more obvious as the propagating wave starts to dominate the electric field. The phase plot in Fig. 7(b) shows the evolution of the dominant electric field from an evanescent wave to a propagating

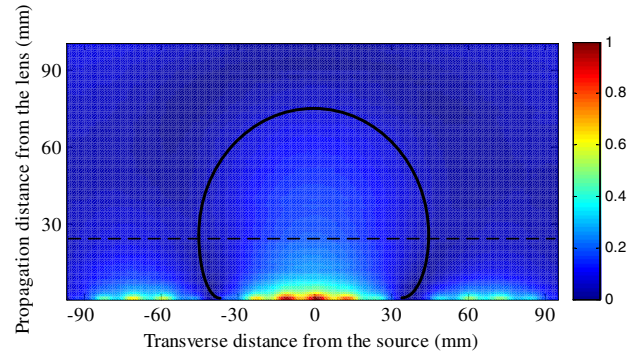


FIG. 6 (color online). The measured magnitude of the vertical electric field detected at the image region at 1.569 GHz. The plot has been normalized to its maximum value. The enhancement of the evanescent waves in magnitude is evident near the exit face of the NRI-TL lens. The dashed line lies at 24 mm away from the rear side of the lens, where the image plane is expected. The solid line demonstrates a magnitude contour plot, of which the phase center lies at the image plane approximately.

wave as the distance increases from 1 to 48 mm. The small ripples observed in the plot when the distance from the lens is small (i.e., 1 mm shown in solid line) are caused by the nonuniform phase distribution along one period (i.e., one unit cell) inside the NRI-TL slab. The measured electric

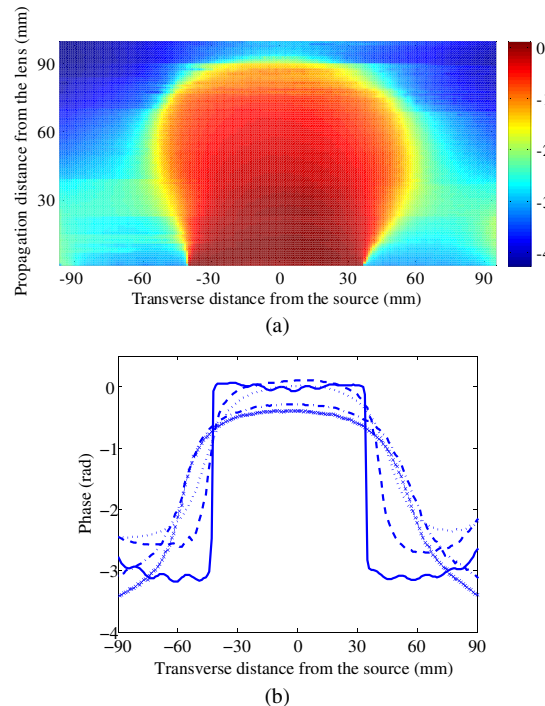


FIG. 7 (color online). The measured phase of the vertical electric field detected at 1.569 GHz. A lack of phase progression is evident near the exit face of the NRI-TL lens where the evanescent waves dominate. (a) shows the phase plot at the entire image region and (b) shows the phase plots at the transverse planes with 1 mm (solid line), 12 mm (dashed line), 24 mm (dotted line), 36 mm (dash-dotted line), and 48 mm (dash-crossed line) away from the lens, respectively.

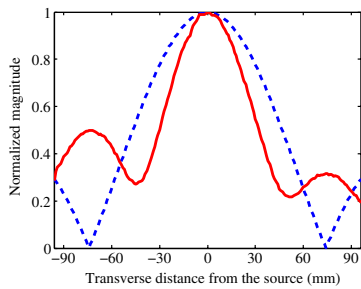


FIG. 8 (color online). The measured vertical electric field (red or gray solid line) along with the diffraction-limited image (blue or dark gray dashed line) at the image plane at 1.569 GHz and at a distance of 24 mm away from the exit surface of the lens. The measured electric field is normalized to its maximum value.

field patterns of the volumetric shunt-node NRI-TL slab lens, shown in Figs. 6 and 7, are similar to those of the planar NRI-TL lens in [11,20], which is consistent with the point of view that this volumetric shunt-node NRI-TL lens is a natural extension of the planar NRI-TL lens of [11]. One important attribute of these plots is that they are dominated by the evanescent components and thus the focusing only takes place in the transverse (and not the longitudinal) plane [11,14,21].

The source is recreated at the image plane at the rear side of the lens. It lies at a distance of 24 mm (two unit cells size, or half of the slab thickness) away from the lens, the same distance with that between the source and the lens for a perfect lens design, as shown in Fig. 6. Figure 8 shows a plot of the normalized electric field at the image plane. It is compared with the diffraction limit for a current line source given by [11,20]

$$E(x) = C \int_{-k_o}^{k_o} \frac{e^{-k_x x}}{k_y} dk_x, \quad (1)$$

where $k_y = \sqrt{k_o^2 - k_x^2}$ and C is a constant that normalizes $E(0) = 1$. The measured half-power beamwidth and null-to-null beamwidth at the image plane are 0.235λ and 0.502λ , respectively, which are significantly narrower than those of a diffraction-limited image ($\sim 0.36\lambda$ and $\sim 0.77\lambda$, respectively). Since the image plane is 0.5λ away from the source, the evanescent wave contribution becomes negligible in a corresponding conventional imaging setup (pertinent diffraction limit) due to the implicated exponential decay. Therefore, this resolution enhancement indicates that the designed volumetric NRI-TL lens has the ability to restore the evanescent waves at the image plane. The plot of the normalized magnitude of the electric field at the rear side of the lens can be found in Fig. 2 of the supplementary material [19], where an increasing beamwidth when moving away from the lens, is observed. This is consistent with the nature of the near-field focusing which is dominated by evanescent waves (see [7,11,14]).

The presented experimental results show that the free space Veselago-Pendry lenses can be realized without

embedded sources and chip elements and is still possible to achieve subdiffraction imaging. Although a single layer NRI-TL lens is presented, thicker lenses can be realized by staking more of those layers upon one another.

We wish to acknowledge the assistance of T. V. Chan in fabricating the parallel-plate waveguide. We also thank M. Stickel, A. Iyer, and A. Grbic for stimulating pertinent discussions [17]. This work was sponsored by the Natural Sciences and Engineering Research Council of Canada.

-
- [1] J. B. Pendry, Phys. Rev. Lett. **85**, 3966 (2000).
 - [2] D. R. Smith, D. Schurig, R. Rosenbluth, S. Schultz, and S. A. Ramakrishna, Appl. Phys. Lett. **82**, 1506 (2003).
 - [3] A. Grbic and G. V. Eleftheriades, IEEE Trans. Antennas Propag. **53**, 3201 (2005).
 - [4] N. Fang, H. Lee, C. Sun, and X. Zhang, Science **308**, 534 (2005).
 - [5] D. Melville and R. Blaikie, Opt. Express **13**, 2127 (2005).
 - [6] M. Wiltshire, Phys. Status Solidi B **244**, 1227 (2007).
 - [7] F. Mesa, M. J. Freire, R. Marquès, and J. D. Baena, Phys. Rev. B **72**, 235117 (2005).
 - [8] A. Salandrino and N. Engheta, Phys. Rev. B **74**, 075103 (2006).
 - [9] Z. Jacob, L. V. Alexseyev, and E. Narimanov, Opt. Express **14**, 8247 (2006).
 - [10] K. Aydin, I. Bulu, and E. Ozbay, Appl. Phys. Lett. **90**, 254102 (2007).
 - [11] A. Grbic and G. V. Eleftheriades, Phys. Rev. Lett. **92**, 117403 (2004).
 - [12] G. V. Eleftheriades, IEEE Microw. Wirel. Compon. Lett. **17**, 412 (2007).
 - [13] P. Alitalo, S. Maslovski, and S. Tretyakov, J. Appl. Phys. **99**, 064912 (2006).
 - [14] A. Grbic and G. V. Eleftheriades, IEEE Trans. Microwave Theory Tech. **51**, 2297 (2003).
 - [15] G. V. Eleftheriades, A. K. Iyer, and P. C. Kremer, IEEE Trans. Microwave Theory Tech. **50**, 2702 (2002).
 - [16] M. Stickel, F. Elek, J. Zhu, and G. V. Eleftheriades, J. Appl. Phys. **102**, 094903 (2007).
 - [17] S. M. Rudolph and A. Grbic, J. Appl. Phys. **102**, 013904 (2007); S. M. Rudolph and A. Grbic, in *Proceedings of the IEEE International Symposium on Antennas and Propagation, Honolulu, Hawaii* (IEEE, Piscataway, NJ, 2007), p. 2542.
 - [18] F. Elek and G. V. Eleftheriades, IEEE Microw. Wirel. Compon. Lett. **14**, 434 (2004).
 - [19] See EPAPS Document No. E-PRLTAO-101-001827 for supplementary material that includes additional information about the nature of the focused fields and the extracted material parameters of the slab. For more information on EPAPS, see <http://www.aip.org/pubservs/epaps.html>.
 - [20] G. V. Eleftheriades and K. G. Balmain, *Negative-Refraction Metamaterials: Fundamental Principles and Applications* (John Wiley and Sons and IEEE Press, New York, 2005).
 - [21] R. Marquès, M. Freiere, and J. D. Baena, Appl. Phys. Lett. **89**, 211113 (2006).